J Appl Electrochem (2009) 39:2061–2072
DOI 10.1007/s10800-009-9913-3

ORIGINAL PAPER

Characterization and corrosion performance of poly(pyrrole-siloxane) films on commercial Al alloys

Monica Trueba · Stefano P. Trasatti

Received: 30 September 2008 / Accepted: 15 April 2009 / Published online: 29 April 2009

Abstract An alternative approach was developed for the surface treatment of as-received commercial aluminium alloys 6082-T6, 5083-H111 and 2024-T3 by using a pyrrole-based silane. One immersion step is sufficient for poly(pyrrole-siloxane) film deposition, with good adhesion and desirable morphological features. The combination in a single coating of polysiloxane linkages, acting as a barrier for aggressive species penetration towards the metal surface, and polypyrrole units manifesting active anodic protection, together with high degree of compactness, explains the significantly improved corrosion protection of the composite film in comparison to simple coatings of polymethylsiloxane and polypyrrole.

Keywords Al alloys · Polysiloxane-based coatings · Polypyrrole · Reflection–absorption infrared spectroscopy · Corrosion protection

1 Introduction

Several alternative technologies for corrosion protection of Al alloys have been investigated in recent years under the urgent need of replacing chromate-based treatments due to toxicity and carcinogenic nature of hexavalent chromium ions. Among the newer approaches explored, electronically conducting polymers (ECPs), particularly polyaniline and polypyrrole, show many potential advantages as corrosion-inhibition coatings, related not only to barrier protection or inhibition, but also to anodic protection [1–3]. Nevertheless, the difficulty of processing due to lack of solubility/fusibility and the low to moderate adhesion constitute the limitations for practical applications. Several approaches have been investigated to improve ECPs processability, such as derivatization of monomer molecules and use of surfactant-like doping ions [4, 5], as well as adhesion by pre-treating Al substrate either mechanically or performing anodic galvanostatic activation before electropolymerization [6, 7]. Parallel to ECPs, silane-based treatments, usually performed by dipping the metal in dilute alcohol or water-based solutions for a short period, have also been intensively studied [8–12]. Among these compounds, organofunctional silanes are most suitable for corrosion protection of various metals and alloys since they provide effective coupling with both metal substrate and organic topcoat [13]. However, silane coatings are likely to be "passive" since they act essentially as a physical barrier by hindering the penetration of aggressive species to the metallic substrate, so that doping with small amounts of chemicals is needed to provide inhibition characteristics [14–16]. At present, no alternative has proven as reliable as chromate for corrosion protection. For successful replacement of chromate-based coatings, it is to bear in mind that chromate treatments not only offer excellent corrosion resistance, including self-healing ability and very good adhesion, but are easily applied.

The present work presents a new alternative for corrosion protection in Al alloys consisting of the use of a pyrrole-based silane (PySi) as a primer. PySi molecule has been used to promote polypyrrole (Ppy) adhesion onto insulating substrates [17–19], although not with reactive metals. If both polypyrrole and polysiloxane were combined in a single coating, a film with improved corrosion protection, chemical/mechanical stability and adhesion should be obtained. Also, simplification of ECPs deposition/processing would be feasible.

M. Trueba (✉) · S. P. Trasatti
Department of Physical Chemistry and Electrochemistry, University of Milan, Via Golgi 19, 20133 Milan, Italy
e-mail: monica.trueba@unimi.it

As-received commercial Al alloys, notably AA6082, AA5083 and AA2024, were modified with PySi following the conventional steps for silanes deposition, i.e., immersion and curing. Poly(pyrrole)-siloxane films (PPySi) were characterized by means of spectroscopic and microscopic techniques. Corrosion performance was evaluated in NaCl solution with various electrochemical and chemical tests. In parallel, polymethylsiloxane (PMeSi) and polypyrrole (Ppy) coatings were also investigated.

2 Experimental

2.1 Materials

Commercially available wrought aluminium alloys (AA), notably 6082-T6, 5083-H111 and 2024-T3, of the nominal composition given in Table 1, were purchased from AVIOMETAL S.p.A. in the form of sheets. Coupons (20 × 30 mm) of 1–1.5 mm thickness depending on the alloy, were cut from the as-received materials. Prior to testing, the specimens were ultrasonically degreased in n-hexane, acetone and methanol, 15 min each.

All chemicals were of analytical reagent grade and used as received, except pyrrole (Py) that was freshly distilled under low pressure and nitrogen atmosphere prior to use. Millipore MilliQ® water was used to prepare solutions.

2.2 Coating deposition

Silane-based coatings, poly(pyrrole-siloxane) PPySi and polymethylsiloxane PMeSi, were obtained by immersion of degreased and pre-heated specimens in hydrolyzed solutions of N-(3-(trimethoxysilyl)propyl)pyrrole or methyltrimethoxysilane, respectively. Solutions were prepared at 4 vol.% in methanol/water (95:5), with pH adjusted to 4 by adding acetic acid (10 vol.%). After immersion specimens were dried in a hot-air stream and cured in an open-to-air sand oven. Multiple immersion/drying steps were performed as listed in Table 2. Coated specimens were kept in a dessicator before experiments.

Polypyrrole films (Ppy) were deposited at room temperature on degreased AA coupons by a two-step procedure [6] as reported in Table 3. The electrochemical apparatus consisted in a mod.553 AMEL potentiostat connected to an one-compartment glass cell with a standard three-electrode configuration. A saturated calomel electrode (SCE) was used as reference electrode and a stainless steel sheet as counter electrode. Cyclic voltammetry experiments were carried out by a mod.1286 Solartron potentiostat in 0.1 mol L^{-1} oxalic acid solution (without monomer) in a single-compartment O-ring cell, properly designed for testing flat working electrode with 1 cm^2 active area [20]. A Pt foil was used as counterelectrode and an external saturated calomel electrode (SCE) as reference electrode. SCE was connected to the working compartment via a salt bridge containing the test solution and a Luggin capillary. All potentials in the text are reported on the SCE scale.

Table 1 Chemical composition (wt%) of commercial wrought Al alloys (AA)

Al alloys	Si	Fe	Cu	Mn	Mg	Zn	Ti	Cr
6082 T6	0.90	0.36	0.04	0.56	1.00	0.02	0.02	0.04
5083 H111	0.17	0.32	0.04	0.62	4.32	0.03	0.02	0.07
2024 T3	0.15	0.25	4.67	0.63	1.34	0.02	0.06	0.01

2.3 Coating characterization

The as-deposited coating of selected samples was identified by reflection–absorption infrared spectroscopy (RAIR), using a FTS-40 Bio-Rad spectrophotometer with a spectral resolution of 4 cm^{-1} and a scan number of 64, in the spectral range 4,000–400 cm^{-1}.

The PPySi coating composition was further analyzed by X-ray photoelectron spectroscopy (XPS) using a ESCA system (XI ASCII Surface Science Instruments) at operating pressure between 10^{-8} and 10^{-9} Torr, fitted with Al anode (1486.6 eV) and 1 eV of energy resolution.

The morphology of the coatings was examined by scanning electron microscopy (SEM), using a 1430 LEO microscope with a chamber pressure of 8 × 10^{-6} Torr and 20 keV accelerating voltage. Sections of the coated substrates were examined after embedding specimen in a cold-working resin, followed by polishing up to 1 μm with diamond paste in non-aqueous solvent.

2.4 Corrosion tests

The experiments were conducted in naturally aerated 0.6 mol L^{-1} NaCl solution (pH 6.5 ± 0.2).

The electrochemical behaviour of the bare and coated specimens was investigated at room temperature by cyclic anodic potentiodynamic polarization curves with a scan rate of 10 mV min^{-1} after an open circuit equilibration of 10 min. The direction of the scan was reversed as current density reached about 5 × 10^{-3} A cm^{-2} up to complete repassivation. The latter was indicated by the potential at which the current density reaches its lowest anodic value (E_{prot}). For selected samples, E_{corr} (or open circuit potential) was recorded as a function of time for at least 15 h. Measurements were obtained using the same electrochemical apparatus as that employed for cyclic voltammetry experiments.

Table 2 Experimental conditions for silane-based coatings deposition

Substrate pre-heatment	Immersion	Curing	Film designation
120 °C, 20 min	3 min	130–150 °C, 2 h	PMeSi3
120 °C, 20 min	(3 min/drying) × 3	130–150 °C, 2 h	PMeSi3 × 3[a]
60 °C, 20 min	1 min	Room T, 24 h	PPySi1*
120 °C, 20 min	1 min	130–150 °C, 1 h	PPySi1
120 °C, 20 min	3 min	130–150 °C, 2 h	PPySi3
120 °C, 20 min	(1 min/drying) × 3	130–150 °C, 1 h	PPySi1 × 3[a]
120 °C, 20 min	(3 min/drying) × 3	130–150 °C, 2 h	PPySi3 × 3[a]

[a] Multiple immersions in silanes hydrolyzed solutions

Table 3 Experimental conditions for Ppy electropolymerization

Steps	Working solution	Current density (mA cm^{-2})	Time (min)
(1) Galvanostatic activation (GA)	0.1 mol L^{-1} Py/0.1 mol L^{-1} HNO_3	24	2
(2) Galvanostatic deposition (GD)	0.8 mol L^{-1} Py/0.1 mol L^{-1} oxalic acid	2	40

Long-term immersion tests were performed on bare and PPySi3 coated specimens at room temperature for a period of 7 days, according to ASTM G31 recommendations [21].

3 Results and discussion

3.1 Polymethylsiloxane films (PMeSi)

PMeSi films deposited on Al appeared not uniform at naked eye, indicating poor wetting of the metal surface by the MeSi hydrolyzed solution. A typical SEM observation of the cross-section of the PMeSi3 film reveals that the film, whose thickness is about 10 μm, appears as a non-continuous layer of solid micro-particles with a rounded shape (Fig. 1). RAIR spectra were similar presenting a shoulder at ca. 1,120 cm^{-1} and a peak at 1,015 cm^{-1}, both characteristic of siloxane antisymmetric stretching vibrations [22–24]. These spectral features indicate small and long chains of linear polysiloxanes.

Single-cycle anodic polarization curves for the PMeSi/AA system are shown in Fig. 2. Some barrier protection is indicated for PMeSi3 on AA6082 and AA5083 (Fig. 2a, b—dotted lines) by a shift of the passive region towards lower currents with respect to the bare substrate. Nevertheless, the film breakdown occurs at a potential (E_b) close to the pitting potential of the uncoated substrate ($E_b \approx E_{pit} = -750$ mV). Higher performance is obtained by multiple deposition (PMeSi3 × 3; dark solid lines) that leads to further lowering of the passive current and to a wider range of passive potentials with a positive shift of E_b of about 200 mV with respect to the bare alloy. The markedly retarded film breakdown, followed by significantly delayed pit propagation, is attributed to both concealment of layer-by-layer defects and increase of film thickness. Further, the potential step or change of slope, observed during the reverse scan of coated substrates, occurs at a potential similar to that of the bare alloys. The above potential was proposed by Yasuda et al. [25] as characteristic of the first stages of Al surface repassivation, and was termed "pit transition potential" (E_{ptp}). Thus, the repassivation process can be considered as determined by the underlying alloy, being less limited for PMeSi3 × 3 than for PMeSi3 according to the position of E_{ptp} at lower current densities and to the less negative E_{prot}. In the case of PMeSi films on AA2024 (Fig. 2c), no protection is obtained as indicated by the almost overlapping polarization curves, which is attributed to poorer adhesion of the coatings on a Cu-rich surface due to lower affinity of copper for silanol group adsorption, that leads to inefficient bonding of siloxane [11, 12].

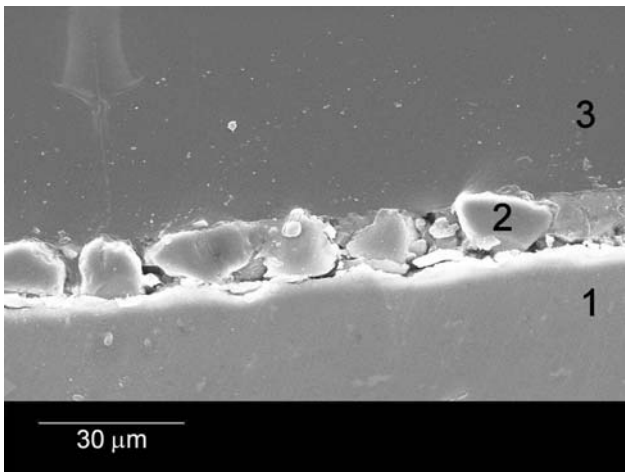

Fig. 1 Cross-section SEM image of PMeSi3/AA6082 (1, metal; 2, coating; 3, mounting resin)

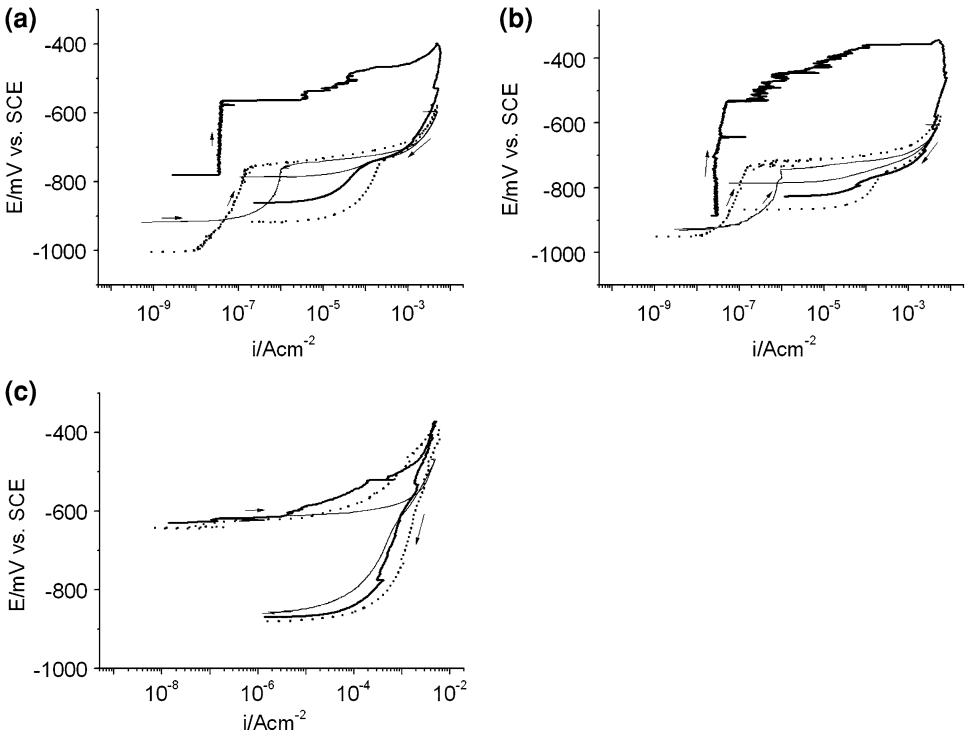

Fig. 2 Single-cycle anodic polarizations ($v = 10$ mVmin^{-1}) of PMeSi films on: **a** AA6082, **b** AA5083, **c** AA2024; in naturally aerated 0.6 mol L^{-1} NaCl (pH 6.5 ± 0.2); (—) bare, (···) PMeSi3, (–) PMeSi3 × 3

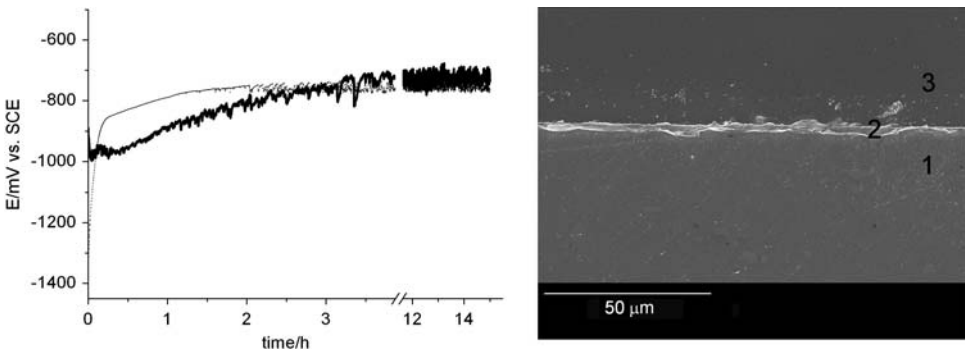

Fig. 3 Potential–time responses of bare (···) and PMeSi3/AA5083 (–) in naturally aerated 0.6 mol L^{-1} NaCl (pH 6.5 ± 0.2). Inset show cross-section SEM image of the coated sample after the test (1, metal; 2, coating; 3, mounting resin)

The poor performance offered by the PMeSi film obtained by single immersion is confirmed by potential–time curves. E_{corr} of coated substrates almost reproduces that of uncoated alloys throughout the experiment, while an appreciable film deterioration was observed at the end of the experiment. A typical result for PMeSi3 coated AA5083 is shown in Fig. 3.

3.2 Polypyrrole films (Ppy)

3.2.1 Synthesis and characterization

Ppy films were deposited on AA substrates by galvanostatic activation (GA) followed by galvanostatic deposition (GD) (Table 3). During the GA step, formation of pits filled with polymer is observed, as indicated in Fig. 4a for AA6082 by black spots. The SEM micrograph of the cross section of the same specimen after the galvanostatic deposition step (GD) (Fig. 4b), confirms this observation and reveals an amorphous, compact film of ca. 10 µm thickness. SEM examination of the film surface indicates globular morphology. However, the polymer growth is more limited on AA6082, reproducing the morphology of the underlying alloy (Fig. 4c). Conversely, Ppy on copper-rich AA2024 apparently surmounts randomly localized pits (Fig. 4d). Both morphologies were observed with PPy/AA5083.

The redox capacity of Ppy/AA system, the dopant presumably being hydrogen oxalate anion [6], is shown in Fig. 5. The irregular reduction pattern (dashed line) with two reduction peaks and no re-oxidation signal, was avoided by allowing the system to conformationally relax at open circuit for 15 min in the electropolymerization

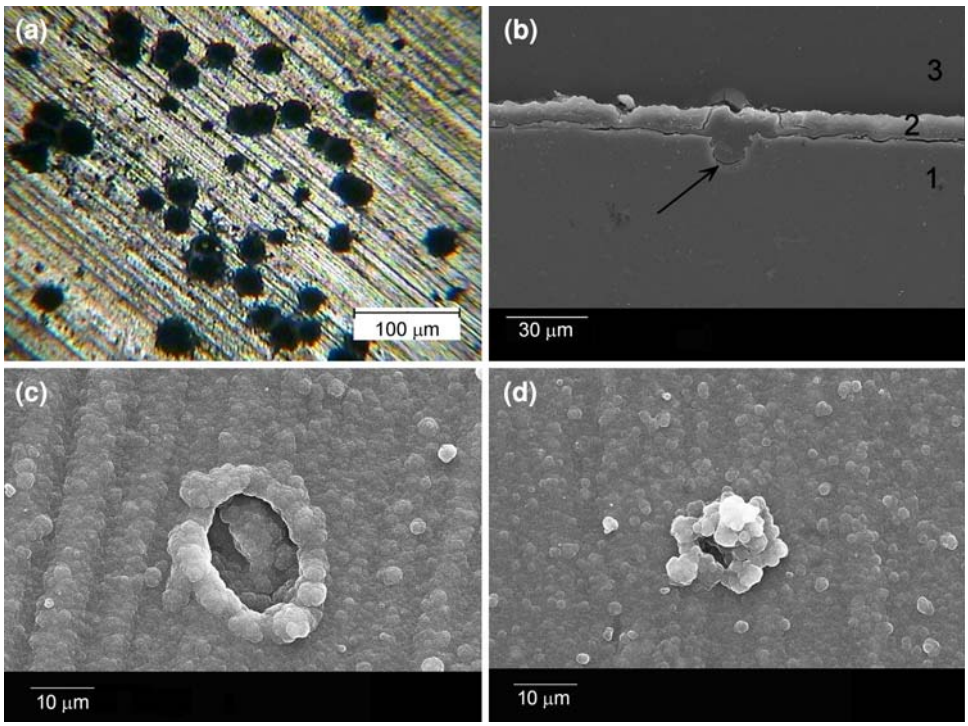

Fig. 4 **a** optical image of AA6082 after galvanostatic activation (GA); **b** cross-section SEM image of Ppy/AA6082, the arrow points the polymer-filled pit; **c, d** surface SEM examination of Ppy-coated AA6082 and AA2024, respectively (1, metal; 2, coating; 3, mounting resin)

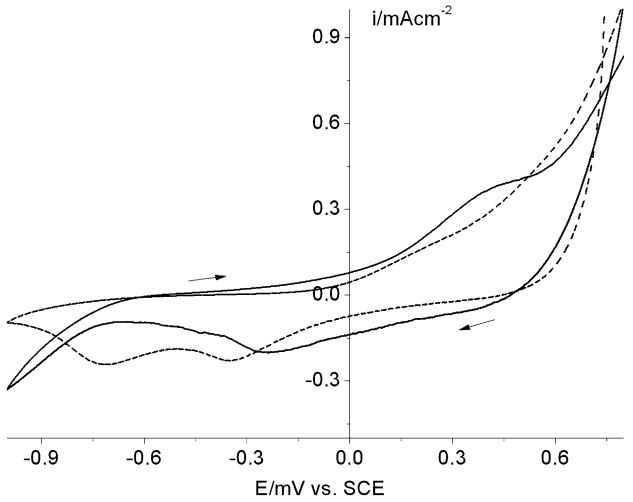

Fig. 5 Typical redox behavior of Ppy film deposited on AA substrates: (- - -) as-prepared Ppy/AA, (—) Ppy/AA after 15 min under open circuit conditions in the electropolymerization media

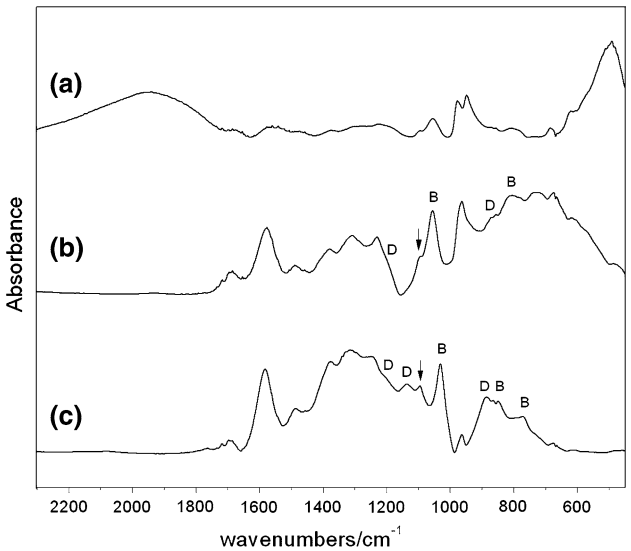

Fig. 6 Reflection–absorption spectra of Ppy films on (a) AA6082, (b) AA5083, (c) AA2024

solution [26] (solid line). The doping degree (y) was determined from the first discharge according to [6]:

$$y = \frac{2Q_d}{(Q_s - Q_d)}$$

where Q_s is the charge consumed during Ppy electrodeposition, and Q_d that released in the first discharge (or reduction). In all cases "y" was <0.2, despite film relaxation that should improve polymer conjugation.

The structural features of Ppy/AA6082 as revealed by RAIR spectroscopy (Fig. 6a) explain the above result. The broad band between 2,300 and 1,700 cm^{-1} in the spectral range of OH absorption, as well as the intense ring deformation at 950 cm^{-1} and N–H wag mode at ca. 490 cm^{-1}, indicate that the polymer chains consist principally of hydroxipyrrolidines and partially saturated pyrrolidines [27, 28]. These functionalities, probably resulting from

acid-catalyzed degradation reactions during Py electropolymerization in the aqueous synthesis medium [29–31], disrupt Ppy conjugation resulting in a less doped polymer.

Similar reasoning cannot be applied to Ppy/AA5083 and Ppy/AA2024 that exhibit higher quality film structure (Fig. 6b, c). Besides clearly resolved Py ring vibrations between 1,600 and 1,200 cm^{-1}, several intense vibration modes of bulk units and doping-induced features are observed (labelled as B and D, respectively) [32–34]. Polymer protonation is suggested by the features near 1,095 cm^{-1} of $N^{+}H_2$ deformation [35] (pointed by arrows in Fig. 6b, c), which would explain the low doping level as a consequence of partial chain saturation [29]. However, it is clear that under similar synthesis conditions degradation reactions are suppressed compared with Ppy/AA6082. The above finding suggests Py ring stabilization by metallic ions released during electropolymerization, more favoured as the reaction is carried out on AA2024 due to polymer doping with stable copper hydrogen oxalate complex (in acidic media) [36–40]. Doping via complex organometallic species (difficult to expel during polymer discharge), would require chains rearrangement for charge compensation maybe involving self-doping via protonation/deprotonation. This could also justify the low value of y, as well as the difference in Ppy structure as a function of the underlying alloy nature. It has been reported for the doping of Pani that metal-oxalate complexes strongly interacting with the polymer produce additional features in the IR spectra as a result of increased conjugation of the polymer chain [41].

3.2.2 *Corrosion performance*

Figure 7 shows the single-cycle polarization curves for Ppy-coated AA5083, AA6082 and AA2024. Differently from PMeSi films, no passive region is observed at the beginning of the polarization, but a positive shift of the forward scan with an exponential current increase. Such observation suggests that the Ppy film does not behave as a simple barrier against aggressive species, but reflects anodic protection. Ppy corrosion is typically associated to the so-called "ennobling" mechanism [42–44], where the polymer provides anodic galvanic protection by keeping the metal passive at small defects or acting as an oxidizer, thus improving the oxide layer at the metal/Ppy interface. The "anodic activity" is further suggested for Ppy/AA6082 (Fig. 7a) by a sequence of rapid current rises, each separated by a region of current stabilization before complete film breakdown. This reveals metastable-like (macro)pitting [45] that indicates Al oxide film regeneration within defects (oxide film healing), possibly favored by Ppy repairing effect. This is also indicated by the semipassivation region at ca. 10^{-4} A cm^{-2} for Ppy/AA2024 in Fig. 7c. The ennobling behaviour observed in the forward scans for Ppy/AA points out that corrosion protection increases in the order AA5083 < AA2024 < AA6082. The

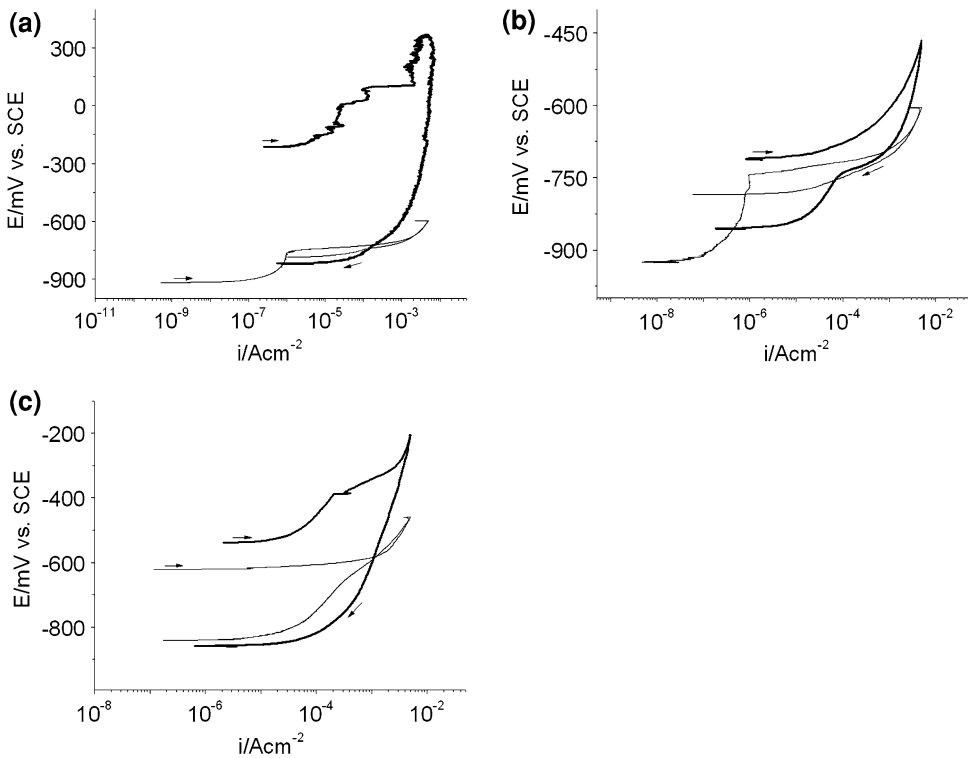

Fig. 7 Single-cycle anodic polarizations ($v = 10$ mVmin^{-1}) of Ppy films on: **a** AA6082, **b** AA5083, **c** AA2024; in naturally aerated 0.6 mol L^{-1} NaCl (pH 6.5 ± 0.2); (—) bare, (–) Ppy/AA

reverse scan reveals more difficult repassivation for Ppy/AA5083 as indicated by the more negative E_{prot} with respect to E_{ptp}, this observation being in agreement with the above sequence. In this case, the worse protection indicates that the Ppy performance is affected by poor film adhesion, resulting from Mg dissolution and hydr(oxides) redeposition during polymer electrogeneration.

By considering the structural features of Ppy as a function of AA nature (Fig. 6), the better performance obtained for highly degraded Ppy/AA6082 may appear as contradictory, but in fact suggests that high degree of polymer conjugation does not necessarily imply good corrosion protection. This anomalous finding can be explained if electrochemically induced conformational changes or rearrangement of the polymeric structure are taken into account [46–48]. Ppy films on AA6082, with partly saturated chains, should present lower free volume due to attracting interactions between neighboring "neutral" chains segments, which results in a more compact film compared with those obtained on AA5083 and AA2024.

Consequently, more anodic potentials and/or longer times of anodic polarization are required to generate free volume for penetration of Cl^- aggressive species through the polymer film on AA6082. The extra energy needed to crack this polymer network explains the significant ennobling in the forward scan, the repairing effect being attributed to the coexistence of conducting and insulating zones in the Ppy matrix.

E_{corr} versus time curves (Fig. 8), carried out under diffusion control rather than being driven by electric fields as in polarization scans, support the role of the rate at which conformational changes occur within the polymer matrix. Differently from what indicated by the polarization curves, an inversion of performance order between Ppy/AA6082 and Ppy/AA2024 is observed in Fig. 8a, b. The E_{corr} exponential decay within the first hours is related to conformational rearrangements induced by Cl^- ion penetration and polymer reduction, the latter contributing to the regeneration of the Al oxide layer at the film/metal interface [44]. However, the time needed to reach the rest potential of the bare substrate for Ppy/AA2024 is almost twice that for Ppy/AA6082. Besides, Ppy/AA2024 exhibits some active protection at longer times (after ca. 13 h). SEM examination of the cross-sections of Ppy-coated specimens (insets of Fig. 8) reveals marked undercoating corrosion for Ppy/AA6082, while a well-adhered film with corrosion products inside the polymer-filled pits is observed on AA2024. The nature of the reactions involved in the corrosion protection of Ppy/AA2024 at open circuit is not known, although copper under-potential deposition could be involved [38, 49, 50]. The above finding is in agreement with the work of Epstein et al. [51], who attributed the higher performance of Pani on AA2024, compared to coated AA3003 and Al, to copper extraction from the alloy surface into the polymer film, thus reducing the galvanic coupling between aluminium and copper.

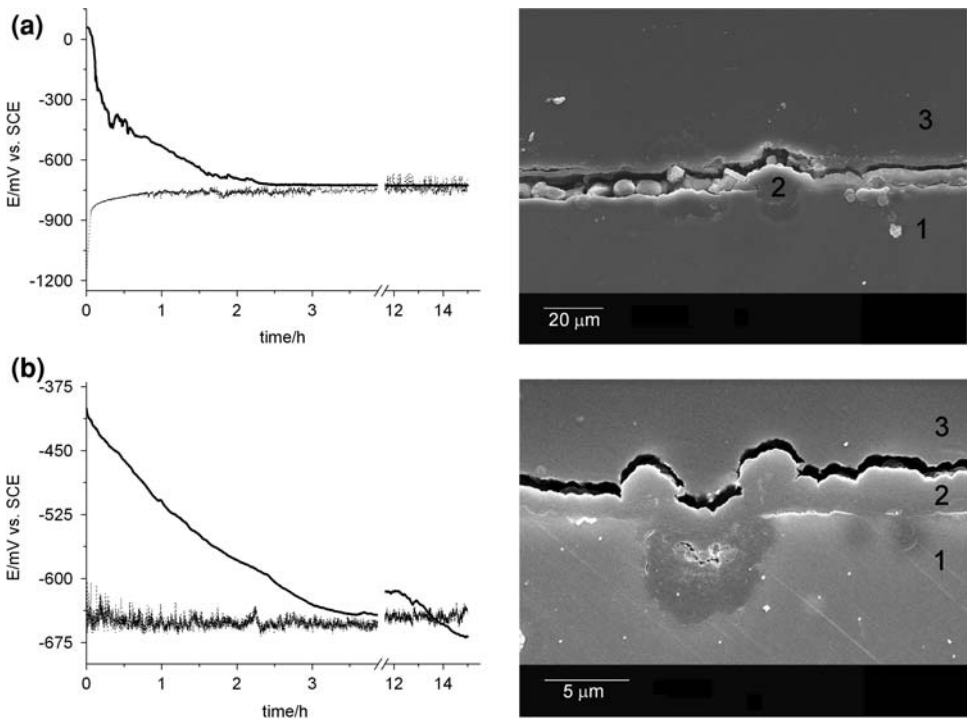

Fig. 8 Potential–time responses of bare and Ppy-coated Al alloys: **a** AA6082, **b** AA2024; in naturally aerated 0.6 mol L^{-1} NaCl (pH 6.5 ± 0.2); (····) bare, (–) PPy/AA. Insets show cross-section SEM images of the corresponding Ppy/AA after the test (1, metal; 2, coating; 3, mounting resin)

Research work is in progress to a better understanding of structural/conformational changes of Ppy linked to corrosion reactions.

3.3 Poly(pyrrole-siloxane) films (PPySi)

3.3.1 Characterization of PPySi films

Good wetting was observed by immersion of AA specimens in PySi hydrolyzed solution, resulting in a homogeneous, thin and transparent film. SEM examination of the cross-section reveals that the thickness is in the range 2–10 μm according to the alloy reactivity, and a well-adhered, closed-packed layer of PPySi is obtained for all the PPySi3/AA systems.

The RAIR spectral features are not influenced by the underlying alloy nature, similarly to PMeSi3/AA, but reflect higher complexity due to the composite structure of the coating that contains both Ppy and polysiloxane chains (Fig. 9) [52]. Conjugated Ppy segments within the composite network are indicated by the polymer characteristic vibrations, bulk units features (B) and doping-induced vibrations (D) [53]. Siloxane stretching vibrations at 1,110 and 1,013 cm^{-1} and the sharp central peak at 1,086 cm^{-1} (pointed by arrows) indicate that polysiloxane units consist of linear chains with cyclic segments of at least 4 units (tetramers) [54]. The tethering of these macromolecules by propyl chains is reflected by C–H vibrations between 2,975 and 2,800 cm^{-1} and a sharp peak at 720 cm^{-1} [55].

Additional XPS characterization supports the composite nature of PPySi (Table 4) but reveals that the surface composition is influenced by the underlying alloy nature. Two nitrogen species are detected for PPySi3/AA2024, i.e., the imine-like (=N−) and positively charged nitrogen (N^+), instead of only pyrrolic nitrogen for PPySi3 on AA6082 and AA5083. These results indicate that copper ions, probably released upon immersion in PySi solution (pH 4), interact with Ppy chains, as migrating out through the composite network [38, 39]. The fraction of positively charged nitrogen [N^+/N] was equal to 0.27, suggesting charge compensation of the Ppy chains due to organometallic complexation. The above Cu–Py interaction, suggested also for Ppy/AA2024, points out the role of the metallic element affinity for coordinating the aromatic Py ring in the polymer chain [36].

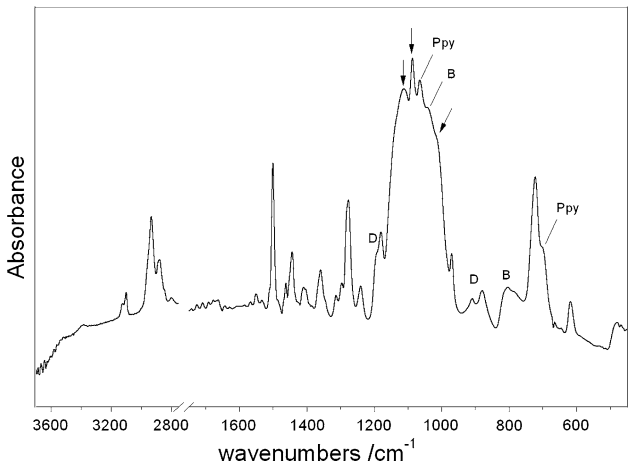

Fig. 9 Reflection–absorption spectra of PPySi3/AA2024

Table 4 Binding energies (eV) and chemical assignments for High-Resolution XPS photopeaks of PPySi3 films on AA6082, AA5083 and AA2024

Photopeak	AA 6082	AA 5083	AA 2024	Chemical assignment
O1s	532.00	531.88	531.88	Si–O
	533.03	533.02		C–O/C=O
N1s			399.16	Imine-like (=N–)
	400.28	400.02		C–N pyrrolic
			401.04	N^+
	284.67	284.70	284.58	C–H, C_β
	285.84	285.57	285.67	C_α/C–N
			286.60	C=N
C1s	286.94			C–O
	287.89	287.59	288.02	C=O
	288.99	289.19		O=C–O
Si2p	102.41	102.27	102.18	C–Si–O

3.3.2 Corrosion performance

The polarization curves for PPySi/AA are shown in Fig. 10. A shift of the passive region towards lower current densities ($\sim 10^{-8}$ A cm^{-2}), accompanied with a wider range of less negative potentials together with a gradual shift of the film breakdown to nobler direction, is obtained as higher preheating and curing temperatures as well as longer immersion times are considered (Table 2). These trends are in agreement with improvement of the corrosion protection behaviour, as a result of higher degree of crosslinking as well as thicker films and defect concealment, as several film layers are deposited on the metal surface. It is to be noted that this behaviour is not influenced by the underlying alloy nature, also in the case of AA2024 (Fig. 10c), where a multiple deposition approach improves significantly the PPySi performance. In addition, the forward scan reveals several "semi-passivation" zones of nearly constant current fluctuations between the pitting potential and the definite breakdown that reflects Al oxide film regeneration within defects, similarly to PPy/AA6082 (Fig. 7a). This observation suggests some repairing effect

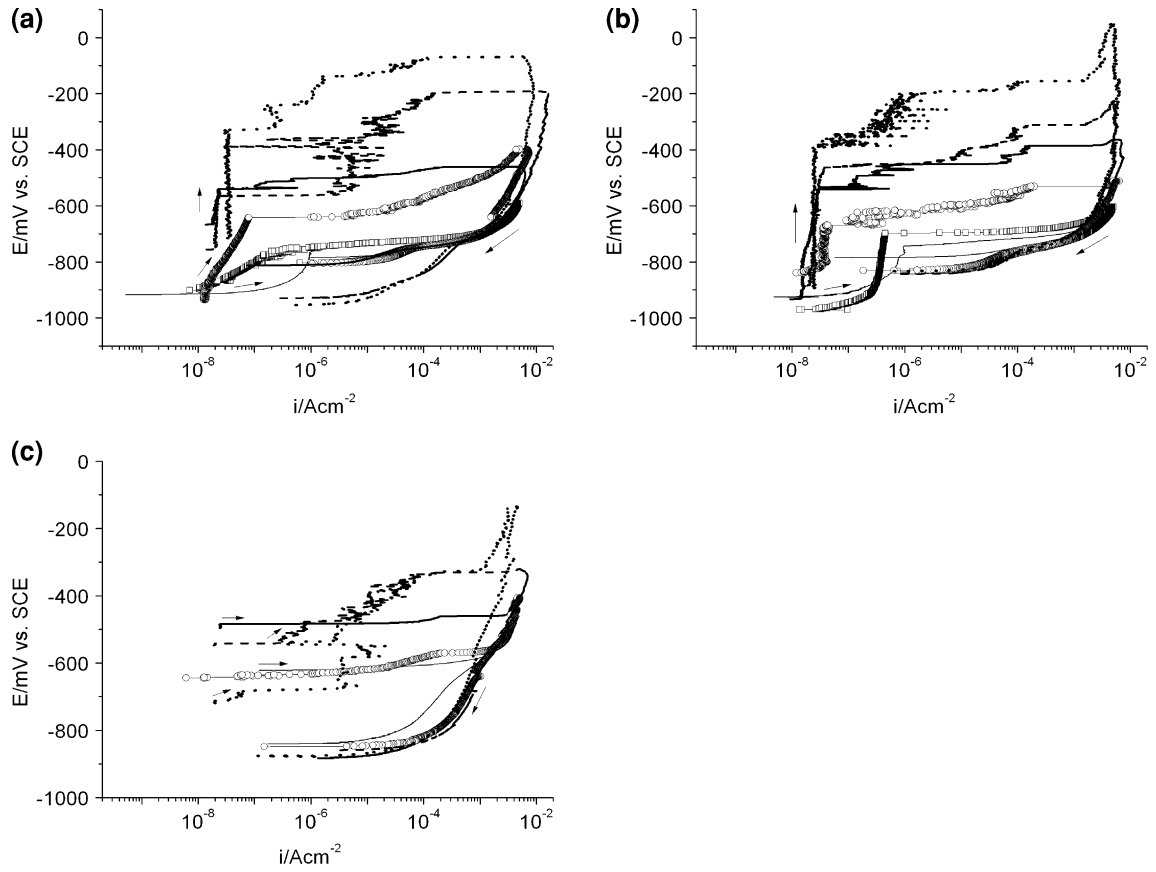

Fig. 10 Single-cycle anodic polarizations ($v = 10$ mVmin^{-1}) of PPySi films on: **a** AA6082, **b** AA5083, **c** AA2024; in naturally aerated 0.6 mol L^{-1} NaCl (pH 6.5 ± 0.2); (—) bare, (□) PPySi1*, (○) PPySi1, (—) PPySi3, (- - -) PPySi1 × 3, (·····) PPySi3 × 3 (see Table 2)

of Ppy moieties within the PPySi film, containing both conducting (Ppy) and insulating (siloxane) regions. In the case of multiple PpySi deposition that leads to thicker films, the above behaviour is expected to be more pronounced as a result of a higher number of active Ppy segments and defect concealment. Hysteresis features are almost independent of the operative conditions (Table 2) and of the degree of ennobling in the forward scan, E_{prot} being not so different from those of the bare alloys, except for PPySi/AA6082. In this case, the hysteresis increases as a multiple-layer approach is used (differently from PMeSi), showing two potential steps, the first at less negative potentials, similar to that observed on the bare substrate although at higher currents, and the second at ca. −900 mV shifted to lower current values. This would suggest coating hindrance affecting repassivation.

The impressive corrosion protection of PPySi as discussed thus far through polarization curves, results from improved film adhesion to the metal surface by siloxane bonding, as well as from its degree of compactness and mixed protection (barrier and anodic actions), due to a composite network of polysiloxane and polypyrrole chains. PMeSi films exhibit a barrier protection mechanism, while Ppy films manifest anodic activity strongly dependent on the underlying alloy that in turn determines the quality of the polymer film.

PPySi composite coatings could be seen as a "reservoir of corrosion inhibitor" in terms of inactive polysiloxane network, containing some conducting Ppy segments that gradually react to avoid metal substrate degradation.

E_{corr} versus time curves for specimens coated by single immersion in PySi solution for 3 min (PPySi3 film) are shown in Fig. 11. The trend of the curves gives further evidence of the higher performance of the composite coating compared with both PMeSi3 and Ppy films. Flat potential transients, initially positive, passing through a maximum and then stabilizing at ca. −850 mV up to the experiment end, characterize both PPySi3/AA6082 and PPySi3/AA5083 systems (Fig. 11a, b). The initial potential decay is attributed to diffusion-controlled conformational changes in the polymer chains within the network [46–48], followed by O_2 reduction at the film surface [56, 57]. Much

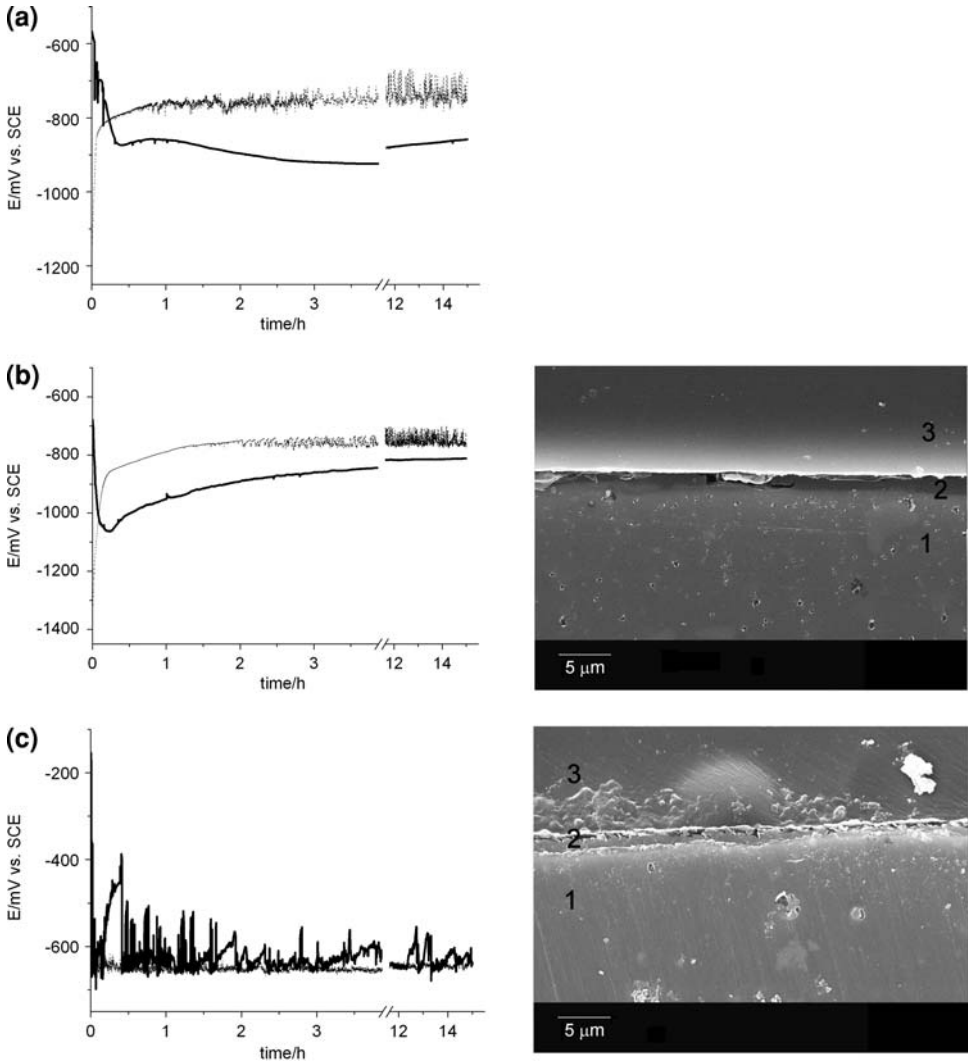

Fig. 11 Potential–time responses for bare and PPySi3-coated Al alloys: **a** AA6082, **b** AA5083, **c** AA2024; in naturally aerated 0.6 mol L^{-1} NaCl (pH 6.5 ± 0.2); (····) bare, (—) PPySi3/AA. Insets in (**b, c**) show cross-section SEM images of the corresponding PPySi3/AA after the test (1, metal; 2, coating; 3, mounting resin)

longer times are needed for film breakdown to occur under these test conditions, which reflects the superior corrosion performance of the PPySi film on these alloys compared to PMeSi (Fig. 3). In the case of PPySi3/AA2024 (Fig. 11c), the potential–time curve shows many transients in the form of marked potential fluctuations mainly positive to the rest potential of the bare substrate. This observation would indicate some repairing effect towards pitting corrosion assisted by Ppy chains within the polymeric network. The potential fluctuations in NaCl solution tend to lower and lower values of both "amplitude" and "intensity" within the first 3 h, occasionally detected for longer times until the end of the experiment. About AA2024, the lower stability of PPySi3 compared with Ppy (Fig. 8), despite the Cu–Ppy entities as indicated by XPS (Table 4), is attributed to a more defective coating as a result of less efficient siloxane bonding to the copper-rich surface. Thus, the performance of PPySi3 on AA2024 is greatly affected as compared to that on AA6082 and AA5083. Cross-section SEM examination of PPySi3/AA at the end of E-t experiments supports the above observation, as shown in the insets of Fig. 11 for AA5083 and AA2024, respectively. Isolated corrosion products and cracks are observed in the PPySi3 film on AA5083 that keeps its amorphous-like nature with a high degree of cohesion and adhesion, while the film on AA2024 appears more damaged. Nevertheless, the failure prevails on the film surface rather than at the film/metal interface with the accumulation of corrosion products on the former, indicating cathodic oxygen reduction dislocation from the metal/film interface, probably assisted by Ppy (and/or Cu–Ppy) moieties within the film. Hence, coating disbondment is diminished.

The promising use of PySi as a primer for corrosion protection of Al alloys was confirmed by long-term immersion tests (7 days) in 0.6 mol L^{-1} NaCl (pH 6.5 ± 0.2), carried out for the PPySi3/AA system [52].

SEM micrographs of the coupon surfaces after immersion tests are shown in Fig. 12. The typical

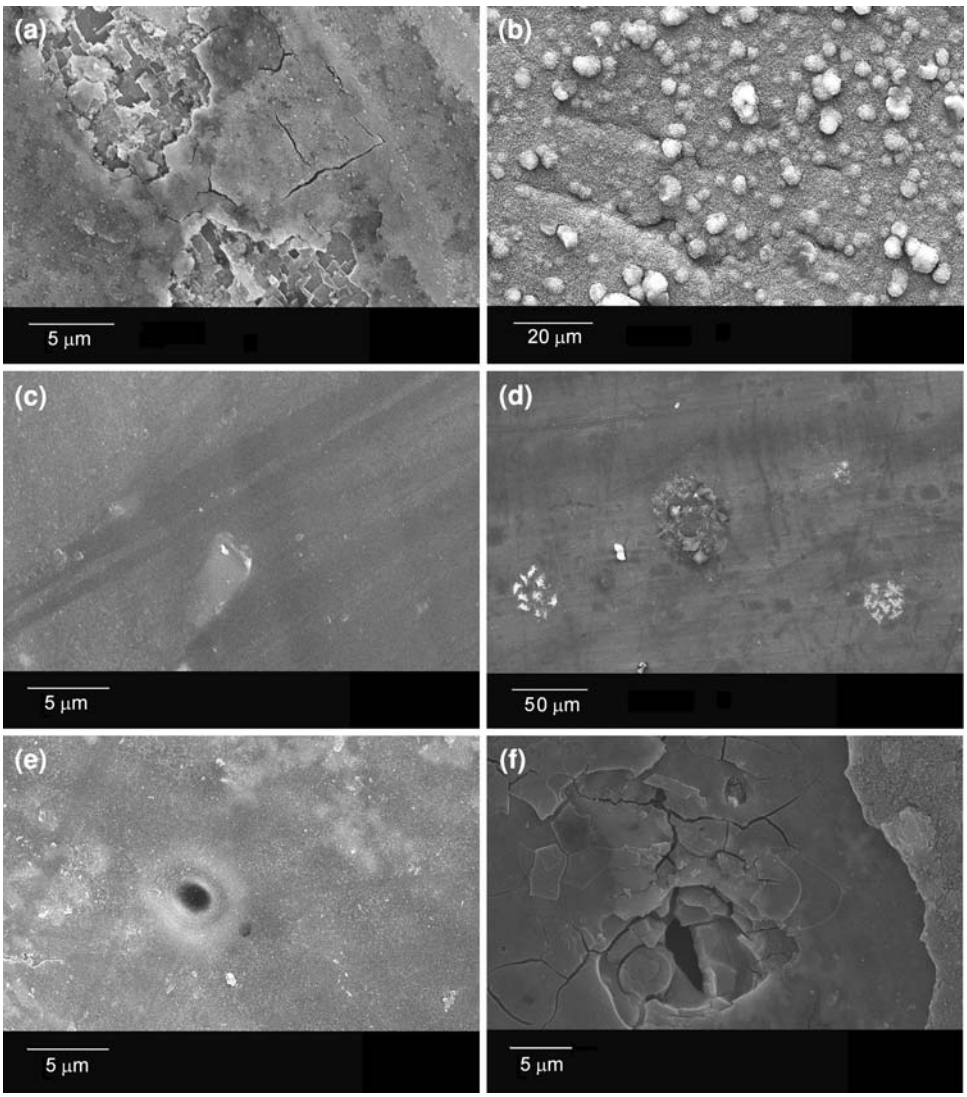

Fig. 12 SEM images of: **a** AA6082, **b** AA5083, **c** PPySi3/AA6082, **d** PPySi3/AA5083, **e** AA2024, **f** PPySi3/AA2024, after 7-days immersion in naturally aerated 0.6 mol L^{-1} NaCl (pH 6.5 ± 0.2)

crystallographic pitting observed on bare AA6082 (Fig. 12a), as well as the roughly circular shape of corrosion products on AA5083 (Fig. 12b), are not observed on the corresponding coated alloys (Fig. 12c, d). The repairing effect of the PPySi3 film keeps AA2024 passive in small-size defects. This effect can be appreciated in Fig. 12e, f.

4 Conclusions

Direct-to metal surface treatment of Al alloys with pyrrole-based silane, following the classical steps for silane deposition, allows to obtain a poly(pyrrole-siloxane) film (PPySi) that contains both polypyrrole and polysiloxane chains. The highly crosslinked network provides an amorphous-like well-packed layer of several microns with improved adhesion. As expected from the original idea that motivated this research work, it is possible to obtain a coating with improved structural/morphological characteristics with respect to simple polymethylsiloxane (PMeSi) and polypyrrole (Ppy) films, via a simplified procedure by using a single molecule that contains both pyrrole and silanol functionalities.

In terms of corrosion protection, the superior performance of PPySi is related not only to its highly cohesive structure and hydrophobic nature, but also to mixed barrier/anodic protection, the former prevailing in PMeSi and the latter in Ppy. In other words, the presence of siloxane chains within the PPySi network improves the adhesion to the metal substrate and contributes to the barrier effect.

Besides, the Ppy segments act as active species against aluminum alloys corrosion throughout the composite matrix. This demonstrates that the main limitations of PMeSi and Ppy are mutually compensated in composite PPySi films.

References

1. Tallman DE, Spinks G, Dominis A, Wallace GG (2002) J Solid State Electrochem 6:73
2. Spinks G, Dominis A, Wallace GG, Tallman DE (2002) J Solid State Electrochem 6:85
3. Zarras P, Anderson N, Webber C, Irvin DJ, Irvin JA, Guenthner A, Stenger Smith JD (2003) Rad Phys Chem 68:387
4. Lee JY, Kim DY, Kim CY (1995) Synth Metals 74:103
5. Ashraf SA, Chen F, Too CO, Wallace GG (1996) Polymer 37:2811
6. Hülser P, Beck F (1990) J Appl Electrochem 20:596
7. Martins JI, Costa SC, Bazzaoui M, Goncalves G, Fortunato E, Martins R (2006) Electrochim Acta 51:5805
8. Petrunin MA, Nazarov AP, Mikhailovski YN (1996) J Electrochem Soc 143:251
9. Johnsen BB, Olafsen K, Stori A, Vinje K (2002) J Adhesion Sci Technol 16:1931
10. Johnsen BB, Olafsen K, Stori A, Vinje K (2003) J Adhesion Sci Technol 17:1283
11. Zhu D, Van Ooij WJ (2003) Corros Sci 45:2163
12. Zhu D, Van Ooij WJ (2003) Corros Sci 45:2177
13. Van Ooij WJ, Zhu D, Palanivel V, Lamar A, Stacy M (2006) Silicon Chem 3:11
14. Osborne JH, Blohowiak KY, Taylor SR, Hunter C, Bierwagon G, Carlson B, Bernard D, Donley MS (2001) Prog Org Coat 41:217
15. Montemor MF, Ferreira MGS (2007) Electrochim Acta 52:7486
16. Palomino LM, Suegama PH, Aoki IV, Montemor MF, De Melo HG (2008) Corros Sci 50:1258
17. Simon RA, Ricco AJ, Wringhton MS (1982) J Am Chem Soc 104:2031
18. Wu CG, Chen CY (1997) J Mater Chem 7:1409
19. Faverolle F, Attias AJ, Bloch B, Audebert P, Andrieux CP (1998) Chem Mater 10:740
20. Murray JN (1997) Prog Org Coat 30:225
21. ASTM G31 – 72 (1999) Standard practice for laboratory immersion corrosion testing of metals, US
22. Thompson WR, Cai M, Ho M, Pemberton JE (1997) Langmuir 13:2291
23. Cai M, Ho M, Pemberton JE (2000) Langmuir 16:3446
24. Angs DL, Simmons GW (1991) Langmuir 7:2236
25. Yasuda M, Weinberg F, Tromans D (1990) J Electrochem Soc 137:3708
26. Krivan E, Visy C, Kankare J (2003) J Phys Chem B 107:1302
27. Park DS, Shim YB, Park SM (1993) J Electrochem Soc 140:609
28. Christensen PA, Hamnett A (1991) Electrochim Acta 36:1263
29. Zhou M, Heinze J (1999) J Phys Chem B 103:8443
30. Sadki S, Schottland P, Brodie N, Sabouraud G (2000) Chem Soc Rev 29:283
31. Patil AO, Heeger AJ, Wudl F (1985) Chem Rev 88:183
32. Tian B, Zerbi G (1990) J Chem Phys 92:3886
33. Tian B, Zerbi G (1990) J Chem Phys 92:3892
34. Zerbi G, Veronelli M, Martina S, Schlüter AD, Wegener G (1994) J Phys Chem 100:978
35. Omastova M, Boukerma K, Chehimi MM, Trchova M (2005) Mater Res Bull 40:749
36. Ruan Ch, Yang Z, Rodgers MT (2007) Phys Chem Chem Phys 9:5902
37. Liu YC, Hwang BJ (1999) Thin Solid Films 339:233
38. Liu YC, Yang KH, Ger MD (2002) Synth Metals 126:337
39. Inoue MB, Nebesny KW, Fernando Q (1990) Synth Metals 38:205
40. Zouaoui A, Stephan O, Carrier M, Moutet JC (1999) J Electroanal Chem 474:113
41. Murugesan R, Subramanian E (2002) Bull Mater Sci 25:613
42. Reut J, Öpik A, Idla K (1999) Synth Metals 102:1392
43. Nguyen TD, Keddam M, Takenouti H (2003) Electrochem Solid State Lett 6:B25
44. Wessling B (1996) Metr Corros 47:439
45. Szklarska Smialowska Z (1999) Corros Sci 41:1743
46. Otero TF, Grande H, Rodriguez J (1997) J Phys Chem B 101:8525
47. Otero TF, Boyano I (2003) J Phys Chem B 107:6730
48. Otero TF, Boyano I (2006) Electrochim Acta 51:6238
49. Liu YC, Hwang BJ (2001) J Electroanal Chem 501:100
50. Liu YC, Chuang TC (2003) J Phys Chem B 107:9802
51. Epstein AJ, Smallfield JO, Guan H, Fahlman M (1999) Synth Met 102:1374
52. Trueba M (2008) Pyrrole-based silane primer for corrosion protection of Al alloys. PhD. Dissertation, University of Milan, Italy
53. McCarley RL, Willicut RJ (1998) J Am Chem Soc 120:9296
54. Parikh AN, Schivley MA, Koo E, Seshadri K, Aurentz D, Mueller K, Allara DL (1997) J Am Chem Soc 119:3135
55. Elmore DL, Chase DB, Liu Y, Rabolt JF (2004) Vib Spectrosc 34:37
56. Kinlen PJ, Silverman DC, Jeffereys CR (1997) Synth Metals 85:1327
57. Schauer T, Joos A, Dulog L, Eisenbah D (1998) Prog Org Coat 33:20